IEEE Access
Multidisciplinary | Rapid Review | Open Access Journal

Received 2 August 2023, accepted 22 August 2023, date of publication 30 August 2023, date of current version 5 September 2023.

*Digital Object Identifier 10.1109/ACCESS.2023.3310432*

RESEARCH ARTICLE

# Frequency Diverse Array Super-Resolution Design With Element Locator Polynomial Rooting Approach

**WEN-QIN WANG, (Senior Member, IEEE)**
Yangtze Delta Region Institute (Huzhou), University of Electronic Science and Technology of China, Huzhou 313001, China
e-mail: wqwang@uestc.edu.cn

This work was supported by the National Natural Science Foundation of China under Grant 62171092.

**ABSTRACT** Unlike traditional phased-array only generating angle-dependent beampattern, the relatively new frequency diverse array (FDA) produces an angle-range-dependent transmit beampattern that can provide many new applications. However, although phased-array physical schemes and characteristics have received much recognition, there still are many open questions about FDA physical schemes and array design. In this paper, we propose an element locator polynomial rooting approach to design super-resolution FDA, where the polynomial is constructed according to the pre-specified FDA levels to enable its roots representing the element locations of the desired FDA. Furthermore, we systematically studies the designed FDA manifold curves for detection and estimation bounds in direction finding. All theoretical results are verified by numerical simulations, which show that FDA outperforms phased-array in terms of detection and resolution thresholds.

**INDEX TERMS** Frequency diverse array (FDA), FDA design, array manifold, array design, manifold curve, super-resolution, differential geometry.

## I. INTRODUCTION

Array manifold is useful in various array signal processing algorithms such as target localization, spectral estimation and array design [1]. Array manifold regards the locus of all array manifold vectors as mathematical objects embedded in multidimensional complex space, which has deep and profound geometric meanings in array applications [2], [3], [4], [5], [6], [7], [8]. Nevertheless, existing publications about array manifold are focused on phased-array [9], [10], [11], [12], [13], [14]. Although phased-array has various important applications, it has only angle-dependent focusing capability and cannot effectively control range-dependent steering. To address this disadvantage, frequency diverse array (FDA) has received much attention in mitigating range ambiguity [15], range-dependent clutter suppression [16] and range-dependent direction modulation [17].

The associate editor coordinating the review of this manuscript and approving it for publication was Cheng Hu.

FDA employs a frequency offset across the array elements to enable its steering direction to change as a function of the space, time and frequency [18], [19], which offers an angle-range-dependent and time-variant transmit beampattern. FDA can be regarded as a combination of spatial diversity and frequency diversity. Nevertheless, FDA is rather different from classic multiple-input multiple-output (MIMO), orthogonal frequency diversion multiplexing (OFDM) and frequency scanning techniques. The comparisons between FDA and other similar array techniques such as phased-array, MIMO, frequency scanning and time-modulated arrays can be found inn the overview articles [18]. FDA multidimensional degrees-of-freedom (DOFs) can be used to resolve range ambiguity and clutter suppression. It is shown that in multipath propagation scenarios, FDA can form a quasi-flat interference pattern for the desired range-angle positions [20], which can be utilized to reduce signal fluctuations. Owing to FDA prospective applications [21], [22], [23], [24], [25], [26], more and more researchers have paid attention to the FDA topic.

However, an important issue that has been overlooked is the investigations on FDA manifold characteristics, which plays a fundamental role in determining the ultimate performance of FDA system. Although phased-array manifold has received much recognition, few studies about FDA manifold can be found. Phased-array manifold curve and surface have been studied in [10], [11], [12], [13], and [14]. But, phased-array manifold only involves the array geometry and steering direction, while FDA extends phased-array manifold to a new manifold that incorporates extra parameters including time, range and frequency offset. We investigated the FDA manifold geometric properties via manifold curve analysis [27] and the FDA manifold geometries for joint angle and range estimation [28]. Nevertheless, there still is a fundamental question: Since the geometry resolution can be higher than the classic array aperture resolution (we call the resolution in manifold geometry as super-resolution), how to deign super-resolution FDA? and what are the performance bound difference between FDA and phased-array? To address this problem, this paper exploits the polynomial rooting approach for phased-array [29] to design super-resolution FDA based on the concept of ''FDA element locator polynomial (FDA-ELP)'' and systematically analyzes the designed FDA detection and estimation performance bounds though the FDA manifold curvatures and coordinate vectors.

Our contributions can be summarized as follows:

1) We propose a polynomial rooting approach to design super-resolution FDA by jointly utilizing FDA-ELP and FDA curvatures. In particular, the design specifications in terms of performance criteria (detection threshold, resolution threshold and Cramér-Rao lower bound (CRLB)) to design fully symmetric FDA are given. Note that in this paper we proposes the approach to optimally design the FDA parameters, which is distinct from our previous paper [28] discussing mainly joint range and angle estimation.
2) The designed FDA detection and resolution thresholds under the FDA manifold curve framework are derived, which validates that FDA outperforms phased-array in detection and resolution capabilities.

The rest of the paper is organized as follows. Section II formulates the FDA manifold curve framework. Sections III proposes the polynomial rooting approach to design super-resolution FDA by jointly utilizing FDA-ELP and FDA curvatures. Next, Section IV derives the designed FDA detection and resolution thresholds under the FDA manifold curve framework. Finally, numerical results are provided in Section V and concluding remarks are given in Section VI.

## II. FDA MANIFOLD CURVE FRAMEWORK

FDA modulates the same baseband waveform to slightly different center frequency for each transmitting element. In doing so, the $m$th element's radiation frequency center is $f_m = f + m\Delta f$, $m = 0, 1, \ldots, M-1$, where $f$ and $\Delta f$ denote the carrier frequency and frequency offset, respectively. Assume a far-field point target located at the angle-range pair $(\theta, r)$. The corresponding FDA manifold steering vector is given by [27]

$$a(\theta, r) = a_\theta(\theta) \odot a_r(r) = e^{j\pi\left(d+\frac{\Delta f}{f}p\odot d\right)\cos(\theta)} \odot e^{-j\frac{2\pi\Delta f}{c}pr} \tag{1}$$

where $c$ is the speed of light. $d = [d_0, d_1, \ldots, d_{N-1}]^T$ and $p = [p_0, p_1, \ldots, p_{N-1}]^T$ are respectively the element position (in half-wavelength) vector and the frequency offset coefficient vector, with $N$ being the number of elements, $d_i$ being the $i$th element position and $p_i$ being the $i$th frequency offset coefficient. $\odot$ and $^T$ denote the Hadamard product and the transpose operator, respectively.

FDA manifold steering vector traces out a surface in the $C^N$, but it is more complex than a curve because FDA manifold steering vector has two free variables, i.e. $(\theta, r)$. Through the families of parameter curves, an alternative representation can be used to simplify the analysis of FDA manifold. Hence, FDA manifold can be treated as families of curves that provide a way to analyze the whole FDA manifold surface. A particularly important family is the FDA $\theta$-curve, which is defined as

$$\Psi = \{a(\theta, r_0), \theta \in [0, \pi)\} \tag{2}$$

with $r_0$ being the target range. For notational simplicity, we use $a(\theta)$ instead of $\mathbf{a}(\theta, r_0)$. Since arc length is a natural parameter to represent the actual physical length in $C^N$, parametrization in terms of the arc length is more suitable. Thus, the arc length $l_{FDA}(\theta)$ of FDA manifold curve can be defined as

$$l_{FDA}(\theta) = \int_0^\theta \|\dot{\mathbf{a}}(\varsigma)\| d\varsigma = \pi \left\|\mathbf{d} + \frac{\Delta f}{f}\mathbf{p}\odot\mathbf{d}\right\| (1-\cos(\theta)) \tag{3}$$

where $\dot{\mathbf{a}}(\varsigma)$ denotes the derivative of $\mathbf{a}(\varsigma)$ with respect to $\varsigma$. For notational convenience, we use $l_{FDA}$ to replace $l_{FDA}(\theta)$, which is the most basic feature of FDA manifold curve. Furthermore, it is an invariant parameter. This means the tangent vector to FDA manifold curve (expressed in terms of $l_{FDA}$) has always a unity norm.

Different from traditional phased-array, the arc length of FDA manifold curve is a function of the angle $\theta$, the element position vector $d$, and the frequency offset coefficient vector $p$. Furthermore, its rate-of-change can be expressed as

$$\dot{l}_{FDA}(\theta) = \|\dot{a}(\theta)\| = \pi \left\|d + \frac{\Delta f}{f}p\odot d\right\| \sin(\theta) \tag{4}$$

Obviously, the rate-of-change provides a useful local property about FDA manifold curve. Applying the chain rule, we get

$$\|a'(l_{FDA})\| = \left\|\frac{da(l_{FDA})}{dl_{FDA}}\right\| = \left\|\frac{\dot{a}(\theta)}{\dot{l}_{FDA}(\theta)}\right\| = 1 \tag{5}$$

where $a'(l_{FDA})$ denotes the derivative of $a(l_{FDA})$ with respect to the arc length $l_{FDA}$. In particular, the total arc length of this

curve (the other important parameter) is

$$l_{m\theta}=2\pi\left\|\mathbf{d}+\frac{\Delta f}{f}\mathbf{p}\odot\mathbf{d}\right\| \tag{6}$$

With the use of (3) and (6), the angle $\theta$ can be expressed as

$$\theta = \cos^{-1}(1-\frac{2l_{FDA}}{l_{m\theta}}) \tag{7}$$

Then, $a(\theta)$ can be rewritten as

$$\mathbf{a}(l_{FDA}) = e^{j\pi\left(\mathbf{d}+\frac{\Delta f}{f}\mathbf{p}\odot\mathbf{d}\right)\left(1-\frac{2l_{FDA}}{l_{m\theta}}\right)}\odot e^{j\gamma} \tag{8}$$

where $\gamma=[\gamma_0,\gamma_1,\ldots,\gamma_{N-1}]^T$ with $\gamma_i = 2\pi p_i\left(-\frac{\Delta f}{c}r_0\right)$, $i=0,1,\ldots,N-1$. We then have

$$\mathbf{a}(l_{FDA}) = \vartheta\odot e^{j\pi\left(\mathbf{d}+\frac{\Delta f}{f}\mathbf{p}\odot\mathbf{d}\right)\left(1-\frac{2l_{FDA}}{l_{m\theta}}\right)} \tag{9}$$

where $\vartheta = e^{j\gamma}$. The derivative of $\mathbf{a}(l_{FDA})$ with respect to the arc length $l_{FDA}$ is

$$u_1(l_{FDA}) = -j\Phi_1\odot\mathbf{a}(l_{FDA}) - j\Phi_2\odot\mathbf{a}(l_{FDA}) \tag{10}$$

where $\Phi_1=\frac{2\pi\mathbf{d}}{l_{m\theta}}$, $\Phi_2=\frac{2\pi\frac{\Delta f}{f}\mathbf{p}\odot\mathbf{d}}{l_{m\theta}}$ and $l_{m\theta}=2\pi\left\|\mathbf{d}+\frac{\Delta f}{f}\mathbf{p}\odot\mathbf{d}\right\|$. Furthermore, the derivative of $u_1(l_{FDA})$ with respect to the arc length $l_{FDA\theta}$ is

$$\begin{aligned}u_1'(l_{FDA}) = &-\Phi_1\odot\Phi_1\odot\mathbf{a}(l_{FDA}) - 2\Phi_1\odot\Phi_2\odot\mathbf{a}(l_{FDA})\\ &-\Phi_2\odot\Phi_2\odot\mathbf{a}(l_{FDA})\end{aligned} \tag{11}$$

Since the first curvature of FDA manifold curve at $l_{FDA\theta}$ is just $k_{1-FDA}=\left\|u_1'(l_{FDA})\right\|$:

$$k_{1-FDA} = \left\|\Phi_1^2+2\Phi_1\Phi_2+\Phi_2^2\right\| \tag{12}$$

where $\Phi_1^2 = \Phi_1\odot\Phi_1$, $\Phi_1\Phi_2 = \Phi_1\odot\Phi_2$, $\Phi_2^2 = \Phi_2\odot\Phi_2$, $\Phi_1=\frac{2\pi\mathbf{d}}{l_{m\theta}}$ and $\Phi_2=\frac{2\pi\frac{\Delta f}{f}\mathbf{p}\odot\mathbf{d}}{l_{m\theta}}$. Thus, the basic properties of FDA manifold curve can be evaluated by the arc length (3), the rate-of-change of arc length (4) and the first curvature (12).

As the curvatures of a manifold curve play an important role in differential geometry, we derive the coordinate vectors of FDA manifold curve and its curvatures. For an $N$-element FDA, its manifold vector can be described by $2N$ real numbers. Moreover, for the FDA having symmetrical elements with respect to its centroid, a curve with $q-1$ nonzero curvatures is embedded in the $q$-dimensional subspace that is within $2N$-dimensional space.

Analogous to [12], we can derive the following recursive equations (derived in *Appendix* A) to obtain the coordinate vectors and curvatures of the FDA manifold curve.

$$\begin{aligned}u_i(l_{FDA}) &= \frac{(j)^i\sum_{n=1}^{\left\lfloor\left(\frac{i-1}{2}\right)+1\right\rfloor}(-1)^{n-1+i}v_{i-1,n}\Phi^{i-2n+2}\odot a(l_{FDA})}{k_{1-FDA}k_{2-FDA}\cdots k_{(i-1)-FDA}}\\ k_i(l_{FDA}) &= \frac{\left\|\sum_{n=1}^{\left\lfloor\left(\frac{i}{2}\right)+1\right\rfloor}(-1)^{n-1+i}v_{i,n}\Phi^{i-2n+3}\right\|}{k_{1-FDA}k_{2-FDA}\cdots k_{(i-1)-FDA}}\end{aligned} \tag{13}$$

where

$$\Phi = \frac{\bar{d}}{\|\bar{d}\|} \tag{14a}$$

$$\bar{d} = d+\frac{\Delta f}{f}p\odot d \tag{14b}$$

$$\sum(\bar{d}) = 0 \tag{14c}$$

Note that, $k_{1-FDA} = \|u_1(l_{FDA})\| = \left\|\Phi^2\right\|$, $k_{(i-1)-FDA}\neq 0$ for $i\geq 2$, $\Phi^i = \underbrace{\Phi\odot\cdots\odot\Phi}_{i}$ and $\lfloor\cdot\rfloor$ denotes the round down operator. The coefficients $v_{i,n}$ are derived as

$$v_{i,n} = \sum_{m_1=1}^{i-2n+3}\sum_{m_2=2+m_1}^{i-2n+5}\cdots\sum_{m_{n-1}=2+m_{n-2}}^{i-1}\begin{pmatrix}k_{m_1-FDA}^2k_{m_2-FDA}^2\\ \cdots k_{m_{n-1}-FDA}^2,\end{pmatrix} \tag{15}$$

where $i,n>2$, $v_{i,1}=1$ *for* $i\geq 1$ and $v_{i,2}=\sum_{m=1}^{i-1}k_{m-FDA}^2$ for $i>1$. That is,

$$v_{i,n} = v_{i-1,n}+k_{(i-1)-FDA}^2v_{i-2,n-1} \qquad i>2, n>1 \tag{16}$$

with the initial conditions: $v_{i,1}=1$ *for* $i\geq 1$ and $v_{2,2}=k_{1-FDA}^2$. The coefficients $v_{i,n}$ are functions of the FDA manifold curvatures.

## III. SUPER-RESOLUTION FDA DESIGN

Assume that an element at the FDA centroid counts as a symmetric element, recalling (13), we have

$$\left\|\sum_{n=1}^{\left(\frac{q}{2}\right)+1}(-1)^{n-1+q}v_{q,n}\Phi^{q-2n+3}\right\| = 0 \tag{17}$$

where $v_{q,n} = v_{q-1,n}+k_{(q-1)-FDA}^2v_{q-2,n-1}$, $q>2$, $n>1$ with the initial conditions: $v_{q,1}=1$ for $q\geq 1$ and $v_{2,2}=k_{1-FDA}^2$. The function in (17) can be expressed as a $(q+1)$-order polynomial:

$$\begin{aligned}f(\phi) &= \sum_{n=1}^{\left(\frac{q}{2}\right)+1}(-1)^{n-1}v_{q,n}\phi^{q-2n+3}\\ &= \phi^{q+1}-v_{q,2}\phi^{q-1}+v_{q,3}\phi^{q-3}-\cdots+v_{q,\left(\frac{q}{2}\right)+1}\phi\end{aligned} \tag{18}$$

which is characterized by the scalar $\phi$ instead of the vector $\Phi$. Obviously, $\phi=0$ is always its roots. It implies that an element at the FDA centroid does affect FDA ambiguity properties, but has no affects on the FDA manifold length and curvatures. Furthermore, (18) can be rewritten as

$$f(\phi) = \phi^q-v_{q,2}\phi^{q-2}+v_{q,3}\phi^{q-4}-\cdots+v_{q,\left(\frac{q}{2}\right)+1} \tag{19}$$

This expression is referred to as the FDA-ELP.

For an $N$-element FDA with the frequency offset coefficients $p$, given the total arc length $l_{m\theta}$ and all the curvatures $\{k_{1-FDA},k_{2-FDA},\cdots,k_{(q-1)-FDA}\}$, the locations of the

FDA elements (and its mirror image) are then given by (derived in *Appendix* B)

$$d_{a/m}=\frac{l_{m\theta}}{2\pi}x_{a/m}\bigcirc\left(1+\frac{\Delta f}{f}p\right) \tag{20}$$

where $x_a$ and $x_m$ are two subsets of the roots $x$ of the following polynomial:

$$f(\phi)=\phi^q-v_2\phi^{q-2}+v_3\phi^{q-4}-\cdots+v_{(\frac{q}{2})+1} \tag{21}$$

where $v_n=v_{q,n}$, $v_{q,n}=v_{q-1,n}+k^2_{(q-1)-FDA}v_{q-2,n-1}$, $q>2$, $n>1$ with $v_{q,1}=1$ for $q\geq 1$, $v_{2,2}=k^2_{1-FDA}$ and

$$x_a=-x_m \tag{22a}$$
$$x_a\cup x_m=x \tag{22b}$$
$$\|x_a\|=\|x_m\|=1 \tag{22c}$$
$$\sum(x_a)=\sum(x_m)=0. \tag{22d}$$

Note that $\bigcirc$ denotes the Hadamard (element by element) division.

Comparing with traditional phased-array, FDA design problem is more complicated. Since the roots of the FDA-ELP can be partitioned into two overlapping subsets that constitute a partially symmetric FDA, we can design the FDA by using the specified curvatures and total arc length. Given the first curvature $k_{1-FDA}$ and the total arc length $l_{m\theta}$ of FDA manifold curve, a symmetric FDA can be designed as

$$d=\frac{l_{m\theta}}{2\pi}x\bigcirc\left(1+\frac{\Delta f}{f}p\right) \tag{23}$$

where $x$ is the subset of the roots to the following polynomial:

$$f(\phi)=\phi^5-v_2\phi^3+v_3\phi \tag{24}$$

with $v_2=-\frac{1}{2}$ and $v_3=\frac{1}{8}\left(1-2k^2_{1-FDA}\right)$.

## IV. FDA DETECTION AND RESOLUTION THRESHOLDS

Similar to traditional super-resolution direction finding phased-array, we evaluate the following FDA performance metrics: Detection threshold, resolution threshold and CRLB for angle estimation.

### A. DETECTION THRESHOLD

For two targets with the angle-range pairs $(\theta_1, r_1)$ and $(\theta_2, r_2)$, respectively, their powers are denoted respectively by $P_1$ and $P_2$. Assume the number of snapshots $L$ is sufficiently large with additive noise power $\sigma^2$. Analogous to [12], FDA detection threshold can be derived as

$$\Delta\theta_{FDA-det}=\frac{1}{\sqrt{2}\dot{l}_{FDA}\left(\widehat{\theta}\right)}\left(\frac{1}{\sqrt{SNR_1\cdot L}}+\frac{1}{\sqrt{SNR_2\cdot L}}\right) \tag{25}$$

where $\widehat{\theta}=\frac{\theta_1+\theta_2}{2}$, $SNR_1=\frac{P_1}{\sigma^2}$ and $SNR_2=\frac{P_2}{\sigma^2}$.

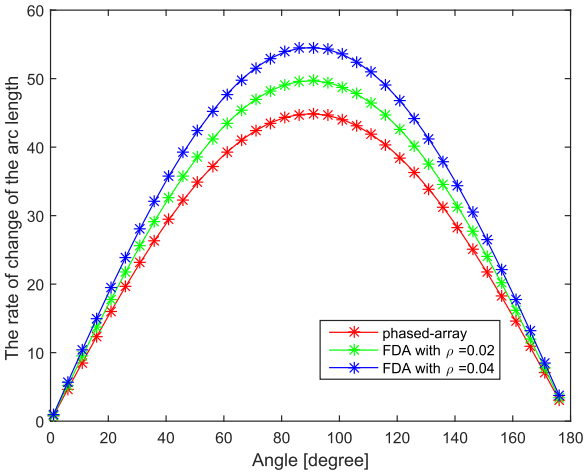


**FIGURE 1.** Rate-of-change of array manifold curve as a function of the angle $\theta$.

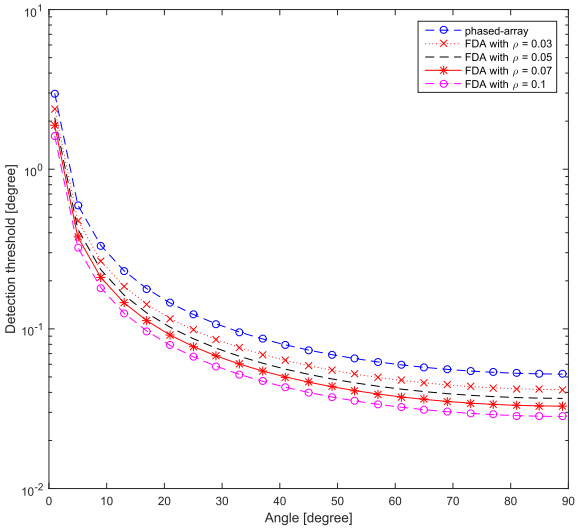


**FIGURE 2.** Comparisons of detection threshold versus angle $\theta$.

We have proved in [28] that, for an $N$-element arbitrary linear array with the frequency offset coefficient $p_i\geq 0, i=0,1,\ldots,N-1$ and at least one of $p_i>0$, we have

$$\dot{l}_{FDA}(\theta)>\dot{l}_{phased-array}(\theta) \tag{26a}$$
$$k_{1-FDA}\dot{l}_{FDA}(\theta)>k_{1-phased-array}\dot{l}_{phased-array}(\theta) \tag{26b}$$

where $\dot{l}_{phased-array}(\theta)$ and $k_{1-phased-array}$ denote the rate-of-change of phased-array manifold curve and the first curvature of phased-array manifold curve, respectively. Thus, it is easily proved that FDA has smaller detection threshold than phased-array, i.e.,

$$\Delta\theta_{FDA-det}<\Delta\theta_{phased-array-det} \tag{27}$$

This implies that FDA outperforms phased-array in detection threshold.

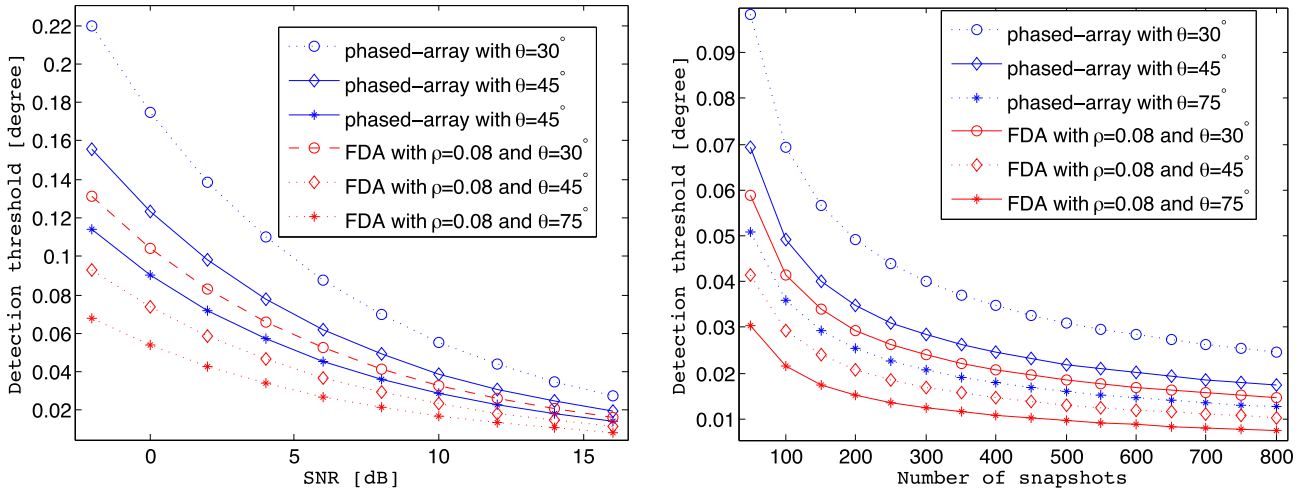


(a) (b)

**FIGURE 3.** Comparisons of detection threshold versus: (a) SNR and (b) number of snapshots.

### B. RESOLUTION THRESHOLD

Similarly, Analogous to [12], the corresponding FDA resolution threshold can be derived as

$$\Delta\theta_{FDA-res} = \frac{1}{\dot{l}_{FDA}\left(\widehat{\theta}\right)} \cdot \frac{\sqrt[4]{2}}{\sqrt[4]{\left(\hat{k}_{1-FDA}^2 - \frac{1}{N}\right)}} \cdot \left(\frac{1}{\sqrt[4]{SNR_1 \cdot L}} + \frac{1}{\sqrt[4]{SNR_2 \cdot L}}\right) \tag{28}$$

where $\hat{k}_{1-FDA} = k_{1-FDA}\sin\left(\chi\left(l_{FDA}\right)\right)$ and $\chi\left(l_{FDA}\right) = \angle\left[u_1\left(l_{FDA}\right), u_2\left(l_{FDA}\right)\right]$. To analyze FDA resolution threshold, we rewrite (28) as

$$\Delta\theta_{FDA-res} = \frac{\sqrt[4]{2}}{\sqrt[4]{\dot{l}_{FDA}^4\left(\widehat{\theta}\right)\left(\hat{k}_{1-FDA}^2 - \frac{1}{N}\right)}} \cdot \left(\frac{1}{\sqrt[4]{SNR_1 \cdot L}} + \frac{1}{\sqrt[4]{SNR_2 \cdot L}}\right) \tag{29}$$

Note that, for a large enough $N$, we have $\hat{k}_{1-FDA}^2 - \frac{1}{N} \approx \hat{k}_{1-FDA}^2$. Then, (29) can be simplified to

$$\Delta\theta_{FDA-res} = \frac{\sqrt[4]{2}}{\sqrt[4]{\dot{l}_{FDA}^2\left(\widehat{\theta}\right)\left(\dot{l}_{FDA}\left(\widehat{\theta}\right)k_{1-FDA}\right)^2}} \cdot \left(\frac{1}{\sqrt[4]{SNR_1 \cdot L}} + \frac{1}{\sqrt[4]{SNR_2 \cdot L}}\right) \tag{30}$$

Due to the fact (26), the following relationship can be obtained:

$$\Delta\theta_{FDA-res} < \Delta\theta_{phased-array-res} \tag{31}$$

This indicates that, for an $N$-element arbitrary FDA with $p_i \geq 0, i = 0, 1, \ldots, N-1$ and at least one of $p_i > 0$, the FDA offers smaller resolution threshold than phased-array.

### C. CRLB

In single and two-target scenarios, the corresponding FDA CRLB can be derived as [27]:

$$\begin{aligned} CRLB_1[\theta_1]_{FDA} &= \frac{1}{2SNR_1 \cdot L \cdot \dot{l}_{FDA}^2\left(\theta_1\right)} \\ CRLB_2[\theta_1]_{FDA} &= \frac{1}{SNR_1 \times L} \\ &\quad \cdot \frac{2}{\dot{l}_{FDA}^2\left(\theta_1\right)(\Delta l)^2\left(\hat{k}_{1-FDA}^2 - \frac{1}{N}\right)} \end{aligned} \tag{32}$$

where $\Delta l = \dot{l}_{FDA}\left(\widehat{\theta}\right)\Delta\theta$, $\hat{\theta} = \theta_1 + \frac{\Delta\theta}{2}$ and $\Delta\theta = \theta_1 - \theta_2$. It shows that FDA outperforms phased-array in angle estimation.

Finally, the performance of FDA and phased array with respect to the detection, resolution and CRLB is summarized as Table 1.

## V. SIMULATION RESULTS

To evaluate the performance between FDA and phased-array, we provide numerical examples to examine the theoretical results.

### A. FDA DESIGN EXAMPLE

Assuming $L = 50$ snapshots and $SNR = 2$ dB, we design a five-element FDA with the following parameters: 1) For a single-target located at $\theta_1 = 30°$, the FDA provides $CRLB_1 = 0.0012°$. 2) For two target scenario, another uncorrelated equipower target is located at $\theta_1 = 34°$, the FDA exhibits $CRLB_2 = 0.0015°$.

Recalling (13), the total FDA arc length and the first curvature are calculated as $l_{m\theta} = 49.1508$ and $k_{1-FDA} = 0.5200$, respectively. Accordingly, the FDA-ELP is $f(\phi) = \phi^5 - 0.5\phi^3 + 0.0573\phi$. Its roots are $\Phi = [-0.5670, -0.42262, 0, 0.4226, 0.5670]^T$. Suppose $p = [2, 1, 0, 1, 2]^T$ and $\rho = 0.005$. The element positions of the

**TABLE 1. Performance comparison between FDA and phased-array under manifold curve framework.**

| Performance | Phased-array | FDA |
|---|---|---|
| $\Delta\theta_{\text{det}}$ | $\frac{1}{\sqrt{2}\dot{l}_{\text{phased-array}}(\widehat{\theta})}\left(\frac{1}{\sqrt{\text{SNR}_1\cdot L}}+\frac{1}{\sqrt{\text{SNR}_2\cdot L}}\right)$ | $\frac{1}{\sqrt{2}\dot{l}_{\text{FDA}}(\widehat{\theta})}\left(\frac{1}{\sqrt{\text{SNR}_1\cdot L}}+\frac{1}{\sqrt{\text{SNR}_2\cdot L}}\right)$ |
| $\Delta\theta_{\text{res}}$ | $\frac{1}{\dot{l}_{\text{phased-array}}(\widehat{\theta})}\cdot\frac{\sqrt[4]{2}}{\sqrt[4]{\left(\hat{k}^2_{1-\text{phased-array}}-\frac{1}{N}\right)}}\cdot\left(\frac{1}{\sqrt[4]{\text{SNR}_1\cdot L}}+\frac{1}{\sqrt[4]{\text{SNR}_2\cdot L}}\right)$ | $\frac{1}{\dot{l}_{\text{FDA}}(\widehat{\theta})}\cdot\frac{\sqrt[4]{2}}{\sqrt[4]{\left(\hat{k}^2_{1-\text{FDA}}-\frac{1}{N}\right)}}\cdot\left(\frac{1}{\sqrt[4]{\text{SNR}_1\cdot L}}+\frac{1}{\sqrt[4]{\text{SNR}_2\cdot L}}\right)$ |
| $\text{CRLB}_1[\theta_1]_{\text{FDA}}$ | $\frac{1}{2\text{SNR}\cdot L\cdot\dot{l}^2_{\text{phased-array}}(\theta)}$ | $\frac{1}{2\text{SNR}\cdot L\cdot\dot{l}^2_{\text{FDA}}(\theta)}$ |
| $\text{CRLB}_2[\theta_1]_{\text{FDA}}$ | $\frac{1}{\text{SNR}_1\times L}\cdot\frac{2}{\dot{l}^2_{\text{phased-array}}(\theta_1)(\Delta l)^2\left(\hat{k}^2_{1-\text{phased-array}}-\frac{1}{N}\right)}$ | $\frac{1}{\text{SNR}_1\times L}\cdot\frac{2}{\dot{l}^2_{\text{FDA}}(\theta_1)(\Delta l)^2\left(\hat{k}^2_{1-\text{FDA}}-\frac{1}{N}\right)}$ |

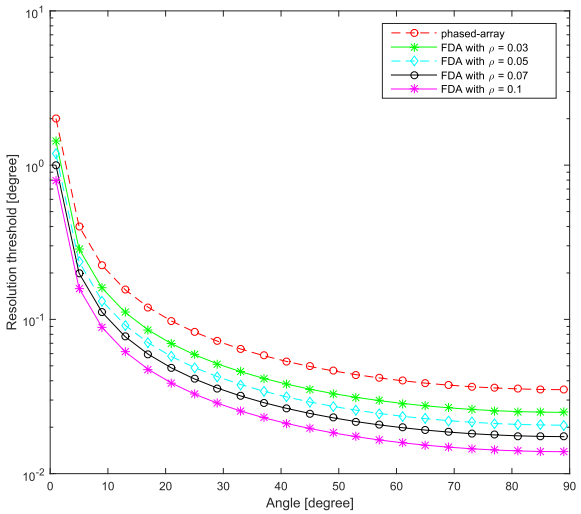


**FIGURE 4. Comparisons of detection threshold versus angle $\theta$.**

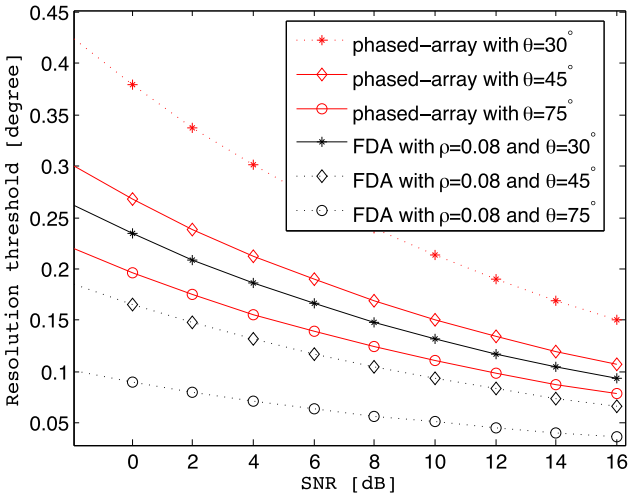


(a)

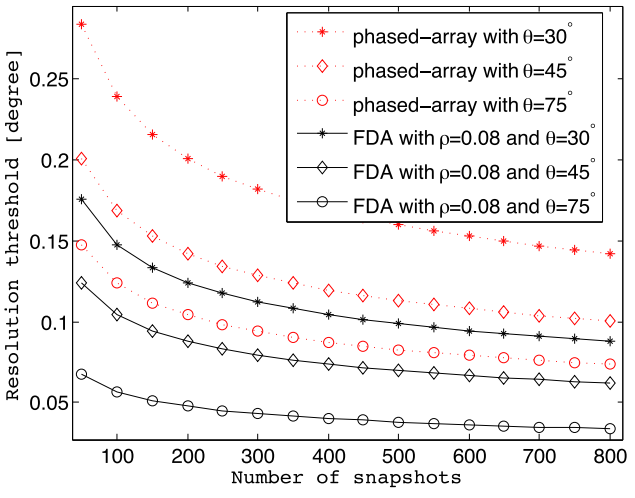


(b)

**FIGURE 5. Comparisons of resolution threshold versus: (a) SNR and (b) number of snapshots.**

required FDA (measured in half-wavelength) are then given by $d = [-4.3915, -3.2895, 0, 3.2895, 4.3915]^T$.

It is important to note that, under the same conditions, a standard five-element FDA has the following CRLB: 1) In single-target scenario, we have $CRLB_1 = 0.0019°$. 2) In two-target scenario, then $CRLB_2 = 0.0030°$.

### B. PERFORMANCE COMPARISON BETWEEN FDA AND PHASED-ARRAY

In order to gain insight into the performance between FDA and phased-array, we compare their the rate-of-change of arc length, detection threshold, resolution threshold and CRLB. For fair comparisons, we use the same reference frequency, i.e.$f = 1GHz$. Note that $\rho = \frac{\Delta f}{f}$ is defined for notational convenience. Note that, when the parameter $\rho = \frac{\Delta f}{f}$ equals to zero, it is just the phased-array.

Firstly, we analyze the rate-of-change of the arc length of FDA manifold curve. Assign the element position (measured in half-wavelength) vector $\mathbf{d} = [1, \ldots, 8]^T$ and the frequency offset coefficient vector $\mathbf{p} = [0, 1, \ldots, 7]^T$. Figure 1 shows that the arc length of FDA manifold curve has larger rate-of-change than that of a phased-array, which is consistent with theoretical analysis. It also indicates that its rate-of-change increases with $\rho$.

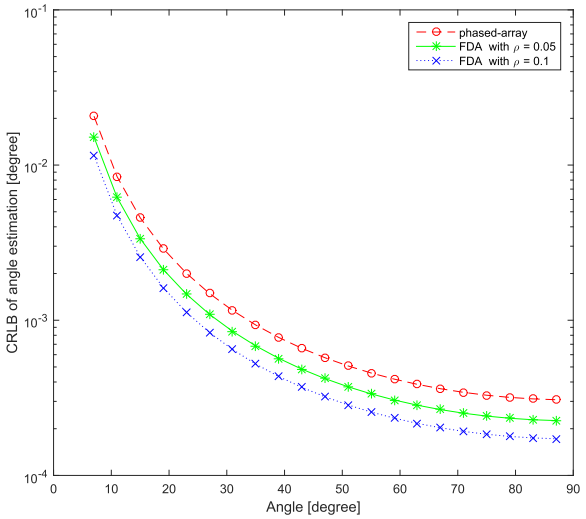


**FIGURE 6.** Comparisons of CRLB for angle estimation versus angle $\theta$ in single-target scenario.

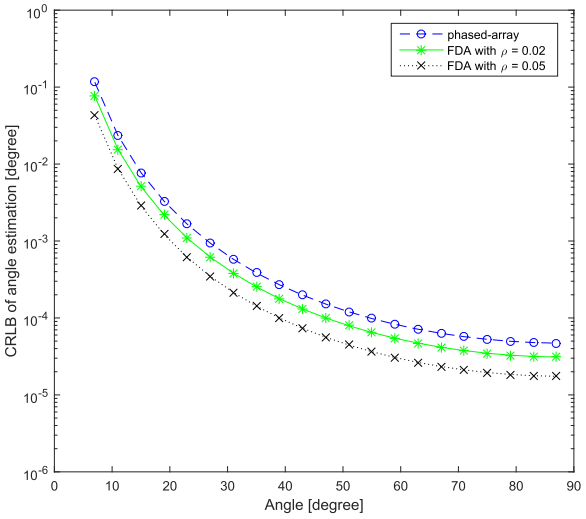


(a)

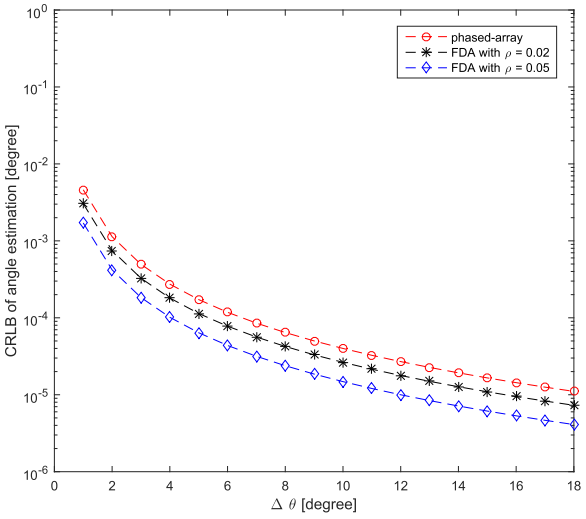


(b)

**FIGURE 7.** Comparisons of CRLB for angle estimation versus: (a) angle $\theta$ and (b) angle difference in two-target scenario.

Secondly, the detection threshold is analyzed. We consider an 11-element linear array with the following parameters: $SNR_1 = 8$ dB, $SNR_2 = 2$ dB, the number of snapshots $L = 50$, $d = [1, 2, 4, 6, 7, 9, 10, 12, 17, 20, 25]^T$ and $p = [0, 1, 2, 3, 4, 5, 6, 7, 8, 9, 10]^T$. Figure 2 depicts the detection threshold with respect to $\theta$. It is seen that FDA outperforms phased-array in detection threshold. With the increase of $\rho$, this difference between FDA and phased-array becomes more obvious. Additionally, we test the detection threshold $\Delta\theta_{FDA-res}$ versus SNR and the number of snapshots. Assume $SNR_1 = SNR_2 = SNR$ with the same other remaining parameters. Note that, in this simulation, the number of snapshots is 50 for Figure 3 (a) and SNR is 5 dB for Figure 3(b). Figure 3 shows that the detection threshold will become smaller with the increase of SNR or number of snapshots. Both Figure 2 and Figure 3 indicate the detection performance can be improved by increasing the angle $\theta$.

Next, we simulate the resolution threshold with the following parameters: $SNR_1 = 8$ dB, $SNR_2 = 2$ dB, $L = 50$, $d = [2, 3, 4, 5, 6, 7, 8, 9, 10, 11, 14]^T$ and $p = [0, 1, 2, 3, 4, 5, 6, 7, 8, 9, 10]^T$. As shown in Figure 4, similar to the detection threshold, FDA produces better resolution threshold than phased-array. It verifies our theoretical results. Furthermore, assume $SNR_1 = SNR_2 = SNR$ with the same other remaining parameters. Let the number of snapshots $L = 50$ for Figure 5(a) and $SNR = 5$ dB for Figure 5(b). Figure 5 indicates that the resolution threshold can be improved by increasing the SNR or the number of snapshots. These results validate that both FDA and phased-array provide finer resolution threshold for a larger $\theta$. More importantly, FDA achieves better resolution threshold than phased-array.

Furthermore, the CRLB for angle estimation is simulated and analyzed. For the single-target scenario, we consider a 5-element standard FDA with element position vector $d = [0, 1, 2, 4]^T$ and frequency offset coefficient vector $p = [0, 1, 2, 3, 4]^T$. Let the number of snapshots be $L = 50$ and $SNR = 8$ dB. In this situation, Figure 6 shows that, for angle estimation, FDA provides lower CRLB than phased-array. The performance difference between FDA and phased-array increases with $\rho$.

Finally, we consider FDA CRLB in two-target scenario. Assume that an array with the element position vector $d = [0, 1, 2, 3, 4]^T$ and the frequency offset coefficient vector $p = [0, 1, 2, 3, 4]^T$, $SNR_1 = SNR_2 = SNR = 8$ dB, the number of snapshots $L = 50$. Note that, Figure 7 (a) $\Delta\theta = 5°$ and Figure 7 (b) the angle of the first target $\theta_1 = 45°$. Figure 7 (a) implies that FDA still outperforms phased-array in DOA estimation. Figure 7(b) gives the CRLB

for angle estimation with respect to the angle difference $\Delta\theta$. It implies that FDA CRLB will decrease with the increase of $\Delta\theta$. Moreover, as shown in Figure 7, FDA CRLB will decrease with the increase of $\rho$. That is, FDA provides better performance in CRLB as the increasing of $\rho$ in two-target scenario. In this situation, the CRLB gap between FDA and phased-array also increases. Thus, its advantage is more obvious.

In conclusion, from the perspective of performance, FDA provides better performance bounds including detection threshold, resolution threshold and CRLB for DOA estimation than conventional phased-array.

## VI. CONCLUSION

As an emerging array technique, FDA has received much attention in radar and communication societies, but FDA manifold curve has not been systematically investigated. In this paper, the curvatures and coordinate vectors of FDA manifold curve were studied systematically. Furthermore, their recursive equations were given, which lead to the FDA-ELP concept. Furthermore, the polynomial rooting approach to super-resolution FDA design was proposed, which is constructed according to the pre-specified FDA performance levels to enable its roots representing the element locations of the desired FDA. Note that the polynomial rooting approach is not limited for the FDA with super-resolution, it also is suitable for other arrays. The FDA performance bounds were also analyzed, which indicates that FDA has better performance than phased-array in detection, resolution and estimation performances. This paper provides a theoretical framework to analyze FDA performance and gives a method to design super-resolution FDA.

## APPENDIX A

Considering the reformulated manifold steering vector expressed in (8), the first coordinate vector of FDA manifold curve can be derived as

$$\begin{aligned} u_1(l_{FDA}) &= a'(l_{FDA}) \\ &= -j\pi\left(d+\frac{\Delta f}{f_0}p\odot d\right)\sin(\theta)\odot da(l_{FDA})\cdot\left(\dot{l}_{FDA}\right)^{-1} \\ &= \frac{-j\pi\left(d+\frac{\Delta f}{f_0}p\odot d\right)\sin(\theta)\odot a(l_{FDA})}{\pi\left\|d+\frac{\Delta f}{f}p\odot d\right\|\sin(\theta)} \\ &= -j\Phi\odot a(l_{FDA}) \end{aligned} \tag{33}$$

where $\Phi=\frac{\bar{d}}{\|\bar{d}\|}$ with $\bar{d}=d+\frac{\Delta f}{f}p\odot d$. Its first curvature is

$$k_{1-FDA} = \left\|u_1'(l_{FDA})\right\| = \left\|\Phi^2\right\| \tag{34}$$

where $\Phi^i=\underbrace{\Phi\odot\cdots\odot\Phi}_{i}$.

Then, the second coordinate vector is

$$\begin{aligned} u_2(l_{FDA}) &= \frac{u'_1(l_{FDA})}{k_{1-FDA}} \\ &= \frac{\left(-j\Phi\odot\left(-j\pi\left(d+\frac{\Delta f}{f}p\odot d\right)\right)\sin(\theta)\odot a(l_{FDA})\right)}{\pi\left\|d+\frac{\Delta f}{f}p\odot d\right\|\sin(\theta)\,k_{1-FDA}} \\ &= \frac{-\Phi^2\odot a(l_{FDA})}{k_{1-FDA}} \end{aligned} \tag{35}$$

We then have

$$\begin{aligned} k_{2-FDA} &= \left\|u'_2(l_{FDA})+k_{1-FDA}u_1(l_{FDA})\right\| \\ &= \left(-\frac{\Phi^2}{k_{1-FDA}}\odot\dot{a}(l_{FDA})\right)\cdot\left(\dot{l}_{FDA}\right)^{-1} \\ &\quad + k_{1-FDA}u_1(l_{FDA}) \\ &= \left\|j\frac{\Phi^3}{k_{1-FDA}}\odot a(l_{FDA})+k_{1-FDA}\left(-j\Phi\odot a(l_{FDA})\right)\right\| \\ &= \frac{1}{k_{1-FDA}}\left\|\Phi^3-k_{1-FDA}^2\Phi\right\| \end{aligned} \tag{36}$$

In the same manner, the third coordinate vector of FDA manifold curve is derived as

$$\begin{aligned} u_3(l_{FDA}) &= \frac{u'_2(l_{FDA})+k_{1-FDA}u_1(l_{FDA})}{k_{2-FDA}} \\ &= j\frac{\left(\Phi^3-k_{1-FDA}^2\Phi\right)}{k_{1-FDA}k_{2-FDA}}\odot a(l_{FDA}) \end{aligned} \tag{37}$$

The third curvature can be expressed as

$$\begin{aligned} k_{3-FDA} &= \left\|u'_3(l_{FDA})+k_{2-FDA}u_2(l_{FDA})\right\| \\ &= \frac{\left\|\varphi^4-\left(k_{1-FDA}^2+k_{2-FDA}^2\right)\varphi^2\right\|}{k_{1-FDA}k_{2-FDA}} \end{aligned} \tag{38}$$

Similarly, we get

$$\begin{aligned} u_4(l_{FDA}) &= \frac{u'_3(l_{FDA})+k_{2-FDA}u_2(l_{FDA})}{k_{3-FDA}} \\ &= \frac{\left(\Phi^4-\left(k_{1-FDA}^2+k_{2-FDA}^2\right)\Phi^2\right)}{k_{1-FDA}k_{2-FDA}k_{3-FDA}}\odot a(l_{FDA}) \end{aligned} \tag{39}$$

$$\begin{aligned} k_{4-FDA} &= \left\|u'_4(l_{FDA})+k_{3-FDA}u_3(l_{FDA})\right\| \\ &= \frac{\left\|\Phi^5-\left(\begin{matrix}k_{1-FDA}^2+k_{2-FDA}^2\\+k_{3-FDA}^2\end{matrix}\right)\Phi^3\right\|}{\left\|+(k_{1-FDA}k_{3-FDA})^2\Phi\right\|} \\ &= \frac{}{k_{1-FDA}k_{2-FDA}k_{3-FDA}} \end{aligned} \tag{40}$$

Then, we assume that

$$\begin{aligned} u_{i-1}(l_{FDA}) &= \frac{(-j)^{i-1}}{k_{1-FDA}k_{2-FDA}\cdots k_{(i-2)-FDA}} \\ &\quad\cdot\sum_{n=1}^{\left\lfloor\left(\frac{i-2}{2}\right)+1\right\rfloor}(-1)^{n-1}v_{i-2,n}\Phi^{i-2n+1}\odot a(l_{FDA}) \end{aligned} \tag{41}$$

and

$$k_{i-1}=\frac{\left\|\sum_{n=1}^{\left\lfloor\left(\frac{i-1}{2}\right)+1\right\rfloor}(-1)^{n-1}v_{i-1,n}\Phi^{i-2n+2}\right\|}{k_{1-FDA}k_{2-FDA}\cdots k_{(i-2)-FDA}} \tag{42}$$

where $v_{i-1,n}$ are given by (15).

To obtain the $i$th curvature, we estimate the term $u'_{i-1}(l_{FDA})$:

$$\begin{aligned}&u'_{i-1}(l_{FDA})\\&=\frac{(-j)^i}{k_{1-FDA}k_{2-FDA}\cdots k_{(i-2)-FDA}}\\&\quad\cdot\sum_{n=1}^{\left\lfloor\left(\frac{i-2}{2}\right)+1\right\rfloor}(-1)^{n-1}v_{i-2,n}\Phi^{i-2n+2}\odot a(l_{FDA})\end{aligned} \tag{43}$$

We then have

$$\begin{aligned}u_i(l_{FDA})&=\frac{u'_{i-1}(l_{FDA})+k_{(i-2)-FDA}u_{i-2}(l_{FDA})}{k_{(i-1)-FDA}}\\&=\frac{1}{k_{1-FDA}k_{2-FDA}\cdots k_{(i-1)-FDA}}\\&\quad\cdot(-j)^i\sum_{n=1}^{\left\lfloor\left(\frac{i-1}{2}\right)+1\right\rfloor}(-1)^{n-1}v_{i-1,n}\Phi^{i-2n+2}\odot a(l_{FDA})\end{aligned} \tag{44}$$

$$\begin{aligned}k_i&=\left\|u'_i(l_{FDA})+k_{(i-1)-FDA}u_{i-1}(l_{FDA})\right\|\\&=\frac{1}{k_{1-FDA}k_{2-FDA}\cdots k_{(i-1)-FDA}}\\&\quad\cdot\left\|\sum_{n=1}^{\left\lfloor\left(\frac{i}{2}\right)+1\right\rfloor}(-1)^{n-1+i}v_{i,n}\Phi^{i-2n+3}\right\|\end{aligned} \tag{45}$$

The (13) can then be derived now.

## APPENDIX B

Assume that $x_a$ and $x_m$ are two subsets of the roots $x_m$ of the following polynomial [29]:

$$f(\phi)=\phi^q-v_2\phi^{q-2}+v_3\phi^{q-4}-\cdots+v_{(\frac{q}{2})+1} \tag{46}$$

Note that its coefficients are functions of the curvatures of FDA manifold curve. Because it only has the even powers, its roots always occur in pairs of opposite signs. For fully asymmetric and partially symmetric FDA, its roots represent two FDA that are mirror images of each other but whose manifold curvatures are identical. Thus, $x_a$ and $x_m$ must satisfy

$$x_a=-x_m. \tag{47}$$

Note that, for fully symmetric FDA, since the FDA and its mirror image are identical, the roots form a single array. Moreover, obviously, $x_a$ and $x_m$ must satisfy

$$x_a\cup x_m=x. \tag{48}$$

Recalling (14a), it implies that $x_a$ and $x_m$ must be normal. That is

$$\|x_a\|=\|x_m\|=1. \tag{49}$$

Besides, (14c) indicates

$$\sum(x_a)=\sum(x_m)=0. \tag{50}$$

From (6), (14a) and (14b), we have

$$\bar{d}_{a/m}=x_{a/m}\left\|d+\frac{\Delta f}{f}p\odot d\right\|=\frac{l_m}{2\pi}x_{a/m}. \tag{51}$$

Therefore, the locations of the elements of the FDA are then given by

$$d_{a/m}=\frac{l_m}{2\pi}x_{a/m}\bigcirc\left(1+\frac{\Delta f}{f}p\right). \tag{52}$$

## REFERENCES


[1] H. So, T. Kaho, Y. Yamamoto, M. Suga, Y. Takahashi, Y. Shirato, and N. Kita, "Staircase array antenna with stacked Butler matrix for concurrent multi-beams," *IEEE Access*, vol. 11, pp. 76638–76646, 2023.

[2] F. Belloni, A. Richter, and V. Koivunen, "DoA estimation via manifold separation for arbitrary array structures," *IEEE Trans. Signal Process.*, vol. 55, no. 10, pp. 4800–4810, Oct. 2007.

[3] B. Friedlander, "Antenna array manifolds for high-resolution direction finding," *IEEE Trans. Signal Process.*, vol. 66, no. 4, pp. 923–932, Feb. 2018.

[4] H. S. Mir, J. D. Sahr, G. F. Hatke, and C. M. Keller, "Passive source localization using an airborne sensor array in the presence of manifold perturbations," *IEEE Trans. Signal Process.*, vol. 55, no. 6, pp. 2486–2496, Jun. 2007.

[5] A. L. Kintz and I. J. Gupta, "A modified MUSIC algorithm for direction of arrival estimation in the presence of antenna array manifold mismatch," *IEEE Trans. Antennas Propag.*, vol. 64, no. 11, pp. 4836–4847, Nov. 2016.

[6] M. Rubsamen and A. B. Gershman, "Direction-of-arrival estimation for nonuniform sensor arrays: From manifold separation to Fourier domain MUSIC methods," *IEEE Trans. Signal Process.*, vol. 57, no. 2, pp. 588–599, Feb. 2009.

[7] Y. I. Wu, K. T. Wong, and S.-K. Lau, "The acoustic vector-sensor's near-field array-manifold," *IEEE Trans. Signal Process.*, vol. 58, no. 7, pp. 3946–3951, Jul. 2010.

[8] M. Costa, A. Richter, and V. Koivunen, "Unified array manifold decomposition based on spherical harmonics and 2-D Fourier basis," *IEEE Trans. Signal Process.*, vol. 58, no. 9, pp. 4634–4645, Sep. 2010.

[9] A. Manikas, H. Commin, and A. Sleiman, "Array manifold curves in $\mathfrak{C}^N$ and their complex Cartan matrix," *IEEE J. Sel. Topics Signal Process.*, vol. 7, no. 4, pp. 670–680, Aug. 2013.

[10] A. Sleiman and A. Manikas, "The impact of sensor positioning on the array manifold," *IEEE Trans. Antennas Propag.*, vol. 51, no. 9, pp. 2227–2237, Sep. 2003.

[11] G. Efstathopoulos and A. Manikas, "Existence and uniqueness of hyper-helical array manifold curves," *IEEE J. Sel. Topics Signal Process.*, vol. 7, no. 4, pp. 625–633, Aug. 2013.

[12] A. Manikas, *Differential Geometry in Array Processing*. London, U.K.: Imperial College Press, 2004.

[13] G. Efstathopoulos and A. Manikas, "Extended array manifolds: Functions of array manifolds," *IEEE Trans. Signal Process.*, vol. 59, no. 7, pp. 3272–3287, Jul. 2011.

[14] A. Manikas, A. Sleiman, and I. Dacos, "Manifold studies of nonlinear antenna array geometries," *IEEE Trans. Signal Process.*, vol. 49, no. 3, pp. 497–506, Mar. 2001.

[15] W. Wan, S. Zhang, and W.-Q. Wang, "Resolving Doppler ambiguity of high-speed moving targets via FDA-MIMO radar," *IEEE Geosci. Remote Sens. Lett.*, vol. 19, pp. 1–5, 2022.

[16] Y. Wang and S. Zhu, "Range ambiguous clutter suppression for FDA-MIMO forward looking airborne radar based on main lobe correction," *IEEE Trans. Veh. Technol.*, vol. 70, no. 3, pp. 2032–2046, Mar. 2021.

[17] H. Xie, H. Ren, Y. Zhang, R. Guo, and H. Liu, "Time frequency direction modulation based on nonlinear frequency diverse array," *IEEE Access*, vol. 11, pp. 32564–32578, 2023.
[18] W.-Q. Wang, H. C. So, and A. Farina, "An overview on time/frequency modulated array processing," *IEEE J. Sel. Topics Signal Process.*, vol. 11, no. 2, pp. 228–246, Mar. 2017.
[19] W.-Q. Wang, "Frequency diverse array auto-scanning beam characteristics and potential radar applications," *IEEE Access*, vol. 10, pp. 85278–85288, 2022.
[20] C. Cetintepe and S. Demir, "Multipath characteristics of frequency diverse arrays over a ground plane," *IEEE Trans. Antennas Propag.*, vol. 62, no. 7, pp. 3567–3574, Jul. 2014.
[21] J. Ma, J. Cai, Z. Zheng, X. Gao, and S. Huang, "Spatiotemporal evolution of orbital angular momentum (OAM) beams based on a uniform circular frequency diverse array (UC-FDA)," *IEEE Trans. Antennas Propag.*, vol. 71, no. 5, pp. 4183–4193, May 2023.
[22] W. Choi, A. Georgiadis, M. M. Tentzeris, and S. Kim, "Analysis of exponential frequency-diverse array for short-range beam-focusing technology," *IEEE Trans. Antennas Propag.*, vol. 71, no. 2, pp. 1437–1447, Feb. 2023.
[23] Y. Liu, R. Zhu, and Q. Liu, "A novel low-cost frequency diverse array with mirrored two-wave mixing," *IEEE Microw. Wireless Technol. Lett.*, vol. 33, no. 3, pp. 359–362, Mar. 2023.
[24] N. Rubinstein and J. Tabrikian, "Frequency diverse array signal optimization: From non-cognitive to cognitive radar," *IEEE Trans. Signal Process.*, vol. 69, pp. 6206–6220, 2021.
[25] W. K. Jia, A. Jakobsson, and W.-Q. Wang, "Designing FDA radars robust to contaminated shared spectra," *IEEE Trans. Aerosp. Electron. Syst.*, vol. 59, no. 3, pp. 2861–2873, Jun. 2023.
[26] L. Wang, W.-Q. Wang, and H. C. So, "Covariance matrix estimation for FDA-MIMO adaptive transmit power allocation," *IEEE Trans. Signal Process.*, vol. 70, pp. 3386–3399, 2022.
[27] T. Liao, Y. Pan, and W.-Q. Wang, "Generalized linear frequency diverse array manifold curve analysis," *IEEE Signal Process. Lett.*, vol. 25, no. 6, pp. 768–772, Jun. 2018.
[28] T. Liao, W.-Q. Wang, J. Xu, and Z. Zheng, "Manifold studies of FDA geometries for joint angle and range estimation," *Signal Process.*, vol. 170, May 2020, Art. no. 107438.
[29] N. Dowlut and A. Manikas, "A polynomial rooting approach to super-resolution array design," *IEEE Trans. Signal Process.*, vol. 48, no. 6, pp. 1559–1569, Jun. 2000.

**WEN-QIN WANG** (Senior Member, IEEE) received the B.E. degree in electrical engineering from Shandong University, Shandong, China, in 2002, and the M.E. and Ph.D. degrees in information and communication engineering from the University of Electronic Science and Technology of China (UESTC), Chengdu, China, in 2005 and 2010, respectively.

From March 2005 to 2007, he was with the National Key Laboratory of Microwave Imaging Technology, Chinese Academy of Sciences, Beijing, China. Since September 2007, he has been with the University of Electronic Science and Technology of China, where he is currently a Professor. From June 2011 to May 2012, he was a Visiting Scholar with the Stevens Institute of Technology, Hoboken, NJ, USA. From December 2012 to December 2013, he was a Hong Kong Scholar with the City University of Hong Kong, Hong Kong. From January 2014 to January 2016, he was a Marie Curie Fellow with Imperial College London, U.K. His research interests include signal processing for radar, communications, and microwave remote sensing. He was a recipient of the Marie Curie International Incoming Fellowship, the National Young To-Notch Talent of the Ten-Thousand Talent Program Award, and the Hong Kong Scholar Fellowship. He is an editorial board member of four international journals.